RSC Advances

ROYAL SOCIETY OF CHEMISTRY

www.rsc.org/advances

Cite this: DOI: 10.1039/c0xx00000x

www.rsc.org/xxxxxx

ARTICLE TYPE

Preparation of Novel Carbon Nanofibers with BiOBr and AgBr Decorating for Photocatalytic Degradation of Rhodamin B

Guohua Jiang,*[a,b,c] Zhen Wei,[a] Hua Chen,[a] Xiangxiang Du,[a] Lei Li,[a] Yongkun Liu,[a] Qin Huang [a] and Wenxing Chen[a,b,c]

Received (in XXX, XXX) Xth XXXXXXXXX 20XX, Accepted Xth XXXXXXXXX 20XX
DOI: 10.1039/b000000x

Novel carbon nanofibers with BiOBr and AgBr decorating have been prepared by combination of electrospinning, carbonization and solvothermal treatments. The BiOBr/AgBr hybrids were covered and interweaved together on carbon nanofibers to form three-dimensional (3D) open porous structure. The resultant composite carbon nanofibers exhibited high efficient to photocatalytic degrade of RhB in the aqueous solution and convenient to separate from water.

During recent decades, photocatalysis has attracted much attention in environmental restoration as a green and sustainable technology[1]. Compared with other photocatalysts, semiconductor photocatalytic process has shown great potential applications due to its lack of toxicity, low cost, high photocatalytic activity and photostability [2]. The ability of this advanced oxidation technology has been widely demonstrated to remove persistent organic compounds and microorganisms in water. Despite these advantages, the practical applications of semiconductor photocatalysts need to deal with three major disadvantages: (1) photocatalytic nanoparticles are easy to form aggregates to minimize their surface area because of their high surface energy, which is unfavorable for photocatalytic reaction; (2) it is very difficult to separate photocatalytic nanoparticles from treated water by conventional methods (including centrifugation and filtration), which may lead to loss of the photocatalyst and bring about secondary pollution; (3) the conventional semiconductors (e.g. TiO_2 and ZnO) are restricted by their deficient visible light absorption or high recombination rate of the photogenerated carriers. To solve these problems, an ideal way is to grow these photocatalytic nanoparticles with visible light responsive on certain substrates in the form of an ordered film without agglomeration [3]. Aiming at effectively utilizing visible light, a great deal of efforts also has been devoted to the hierarchical structure development and band gap regulation because shape and band energy of photocatalysts play vital influence on their physical/chemical properties [4]. Among of them, bismuth oxyhalide compounds have attracted considerable attention due to their remarkable photocatalytic activities under visible-light illumination [5], and their optical and catalytic properties can be modified by incorporation of other highly reactive component, such as cation, anion, metal oxides and metal nanoparticles [6].

Herein, we report a facile preparation of novel carbon nanofibers with BiOBr and AgBr decorating. Carbon nanofibers are flexible, conductive, and stable in corrosive conditions, and they can supply a large surface area, which is critical for nanostructure-based photovoltaic technology [3c]. They also have good heat and fatigue resistance. Moreover, the synergistic effect of BiOBr, AgBr and carbon nanofibers will greatly retard the recombination of photoinduced electrons and holes, which could significantly enhance photocatalytic performance of hybrid composite nanofibers. Fig. 1 shows a schematic representation of the growth process of a BiOBr/AgBr hybrids on the carbon nanofibers (see detail preparation in ESI). Firstly, a spinning solution containing polyacrylonitrile (PAN) and $BiCl_3$ with N, N-dimethylformamide (DMF) as solvent has been developed to produce composite PAN nanofibers via electrospinning. After the heat treatment, the PAN nanofibers are carbonized to form carbon nanofibers and Bi_2O_3 and Bi nanoparticles are immobilized on the carbon nanofibers due to oxidiation of $BiCl_3$ and reduction of PAN at high temperature (see Fig. S1 and S2 in ESI) [7]. The Bi_2O_3 and Bi nanoparticles immobilized on the carbon nanofibers can be utilized as seeds to growth BiOBr/AgBr hybrids that has stronger photocatalytic ability than that of pure BiOBr [8]. And these BiOBr/AgBr hybrids are further assemblied into hierarchical architectures on the surface of carbon nanofibers by a solvothermal method.

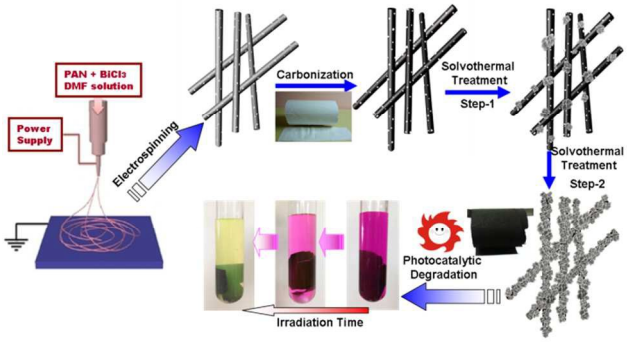

Fig. 1 The schematic representation of the growth process of BiOBr/AgBr hybrid nanosheets on the carbon nanofibers.

The morphology and structure of the carbon nanofibers with BiOBr/Ag hybrids decorating are firstly characterized by field-emission scanning electron microscopy (FE-SEM) and transmission electron microscopy (TEM). The carbonized

composite nanofibers are immersed into the solution of $Bi(NO_3)_3$, $AgNO_3$ and CTAB. After solvothermal treatment at 160°C for 1h, the BiOBr/AgBr hybrids covered on carbon nanofibers can be observed. As shown in Fig. 2A, these isolated BiOBr/AgBr hybrids with flower-like structure are distribuated on the surface of carbon nanofibers. It looks like the plum blossoms on the head of tree branches (inset in Fig. 2A). The size of flower-like BiOBr/AgBr hybrids is around 700 nm. They are consisted of spindle-like nanosheets with ~200 nm in width and ~5 nm in thickness (Fig. 2B). Prolonging the solvothermal treatment time to 6 h, the BiOBr/AgBr hybrids are uniformly and compactly covered to form a rough surface (Fig. 2C and Fig. S3 in ESI). Further magnification of SEM image of as-prepared composite nanofibers, these nanosheets interweaved together to form an open porous structure can be founded (Fig. 2D). It has been reported that such small sizes of these nanosheets may be indicative of a possible quantum confinement effect for the properties of such structures [9]. TEM measurement has been applied to analysis the composition and structure of nanosheets. Fig. 2E shows the TEM image of BiOBr/AgBr hybrid carbon nanofibers. The nanosheets are compactly growth on the surface of carbon nanofibers. Selected area electron diffraction (SAED) patterns taken from the edge of the nanosheets is shown in Fig. 2F. It reveals the obvious lattice spacing of d = 0.28 nm, which is close to the d-spacing of the [102] (0.21 nm) reflections of pure BiOBr [10]. The slight distinction in lattice spacing is deviation due to the presence of dopant. Another lattice spacing of d = 0.33 nm is contributed from the [111] reflections of AgBr[11].

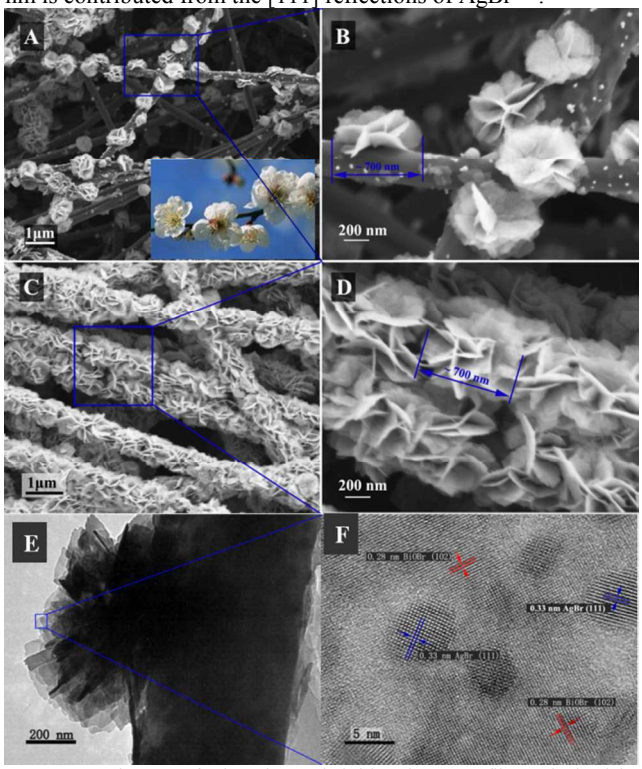

Fig. 2 SEM images of BiOBr/AgBr hybrid carbon nanofibers obtained by solvothermal treatment for 1h (A and B, the photo of plum blossoms on the head of tree branches (inset in A)) and 6 h (C and D). TEM image of BiOBr/AgBr hybrid carbon nanofibers (E) and selected area electron diffraction (SAED) pattern taken from the edge of the nanosheets (F).

The crystallographic structure of the composite nanofibers is further confirmed by powder X-ray diffraction (XRD) analysis. As shown in Fig. 3A, an obvious broad peak with 2θ from 10° to 20° can be observed from carbon nanofibers, which is assigned to amorphous carbon. The diffraction peaks of the carbon nanofibers at 27.2°, 37.2°and 39.3° are in good agreement with the (012), (104) and (110) of hexagonal Bi phase (JCPDS, 85-1329). There also appear some weak and broad additional peaks, which match crystal planes of Bi_2O_3 (JCDPS, 74-1375): (220), (013), (600) and (145) at 2θ = 24.5, 26.0, 53.9 and 56.2 [12]. It indicates the $BiCl_3$ has been reduced and oxidized simultaneously during the carbonization. After solvothermal treatment, the diffraction peaks can be indexed to the tetragonal phase BiOBr (JCDPS, 09-0393, 2θ = 25.2, 32.2 46.2 and 57.1 correspond well to (001), (110), (200) and (212) [13]. The XRD pattern for the BiOBr/AgBr hybrid carbon nanofibers also exhibits some weak dopant related peaks from AgBr (JCDPS, 06-0438) besides the typical tetragonal structure of BiOBr crystal due to the low content and high dispersity of dopants. No diffraction peaks of metal Ag are observed. The X-ray photoelectron spectrum (XPS) of the photocatalyst exhibit prominent peaks of carbon, oxygen, bismuth, bromine and relatively feeble peaks of nitrogen and silver, as shown in Fig. 3B. The high-resolution XPS spectrum of Ag 3d from the composite photocatalyst is shown in Fig. 3C, which can be fitted as two peaks at binding energies of 367.2, and 373.2 eV, respectively, suggesting the presence of AgBr. As for the high resolution XPS spectrum of Br 3d that shown in Fig. 3D, the binding energy of 67.8-68.3 eV and 68.7-69.2 eV can be observed. They are referred to Br $3d_{5/2}$ and $3d_{3/2}$ respectively which can be assigned to Br at the monovalent oxidation state [14]. The overlapped peak of Br 3d at higher binding energy (~68.9 eV) is due to the crystal lattice of Br in AgBr [15]. These results are in agreement with the HR-TEM and XRD analysis.

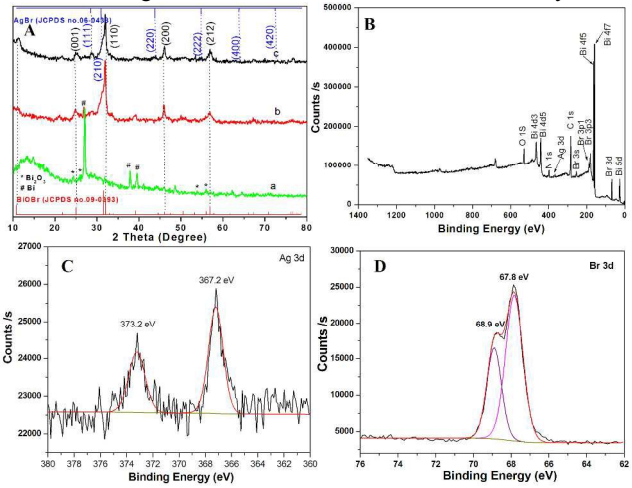

Fig. 3 XRD pattern of carbon nanofibers (A) (a: naked carbon nanofibers, b: BiOBr covered carbon nanofibers, c: BiOBr/AgBr hybrid carbon nanofibers). XPS spectrum of the as-prepared BiOBr/AgBr hybrid carbon nanofibers (B) and high-resolution XPS spectra of Ag 3d (C) and Br 3d over BiOBr/AgBr hybrid carbon nanofibers.

Photoluminescence (PL) analysis was used to reveal the efficiency of charge carrier trapping, transfer, and separation and to investigate the fate of photogenerated electrons and holes in composite carbon nanofibers, because the PL emission results from the recombination of free charge carriers [16]. Herein, we present the suitable PL measurement for carbon nanofibers

covered with BiOBr or BiOBr/AgBr hybrids and physical mixture of carbon nanofibers and BiOBr/AgBr hybrids, as shown in Fig. 4A. A broad PL emission spectrum was observed for all products. However, in comparison with carbon nanofibers covered with BiOBr (curve b), the intensity of the PL signal for the carbon nanofibers covered with BiOBr/AgBr hybrids is much lower (curve a). It indicates that the composite carbon nanofibers have a lower recombination rate of electrons and holes, due to the fact that the electrons are excited from the valence band to the conduction band and then transfer to carbon nanofibers, preventing a direct recombination of electrons and holes. It also implies the electron-hole recombination on the surface of composite carbon nanofibers is largely inhibited to generate more photoelectrons and holes to participate in the photocatalytic reactions [17]. In the case of physical mixture of carbon nanofibers and BiOBr/AgBr hybrids, the intensity of the PL signal is close to the BiOBr/AgBr hybrids (curve c) and much higher than that of composite (curve a). It suggests the carbon nanofibers are not working for acceleration of electron transfer due to no close connection between the carbon nanofibers and BiOBr/AgBr hybrids. The photocurrent responses of carbon nanofibers covered with BiOBr and BiOBr/AgBr hybrids under visible light ($\lambda > 420$ nm), are shown in Fig. 4B. The photocurrent intensity remains at a constant value when the light is on and rapidly decreases to zero as long as the light is turned off. It is obvious to observe that the photocurrent over BiOBr/AgBr hybrid carbon nanofibers is greatly improved, which is about 1.3 times as high as that of BiOBr/AgBr hybrids. Because the photocurrent is formed mainly by the diffusion of photogenerated electrons to the back contact and simultaneously holes are taken up by the hole acceptor in the electrolyte [18]. The enhanced photocurrent over BiOBr/AgBr hybrid carbon nanofibers implies more efficient separation of the photoinduced electron–hole pairs and longer lifetime of the photogenerated charge carriers than that of BiOBr/AgBr hybrids, which is beneficial for its enhanced photocatalytic activity. However, in the case of physical mixture of carbon nanofibers and BiOBr/AgBr hybrids, the photocurrent intensity is lower the composite and close to that of BiOBr (curve c). It further confirms the higher separation efficiency of the photoinduced electron–hole pairs in composite.

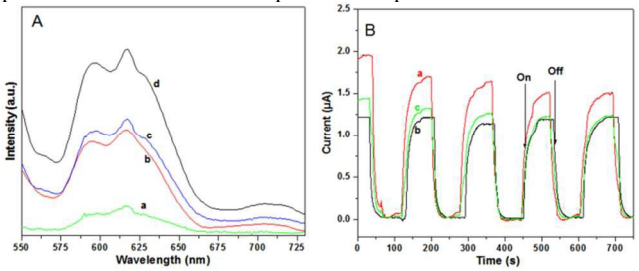

Fig. 4 Room-temperature photoluminescence (PL) emission spectra of composite carbon nanofibers (a: covered with BiOBr/AgBr hybrids, b: covered with BiOBr, c: physical mixture of carbon nanofibers and BiOBr/AgBr hybrids) and pure BiOBr (d) (λ_{ex} = 370 nm) (A) and photocurrent intensity of film electrodes in Na_2SO_4 solution, over carbon nanofibers covered with BiOBr/AgBr hybrids (a), BiOBr (b) and physical mixture of carbon nanofibers and BiOBr/AgBr hybrids (c) under visible light irradiation ($\lambda > 420$ nm, [Na_2SO_4] = 0.1 M) (B).

The photocatalytic activity of the as prepared products was further evaluated by degradation of Rhodamine B (RhB, C_{RhB}= 10 mg/L) under the visible light irradiation. As shown in Fig. 5A. For the comparison, a blank experiment is firstly carried out for indicating the self-photodegradation of RhB. It can be founded the self-photodegradation of RhB is almost negligible under light irradiation without any catalysts. Under the light irradiation, the decolorization rate of RhB can be accelerated in presence of carbon nanofibers, which can be ascribed to the dual actions of photolysis and adsorption [19]. The decolorization rate of RhB is further accelerated in the presence of the BiOBr or BiOBr/AgBr composite photo-catalysts. There is no doubt here that photocatalysis plays an important role to decolor RhB besides photolysis and adsorption. The fastest decolorization rate can be obtained using BiOBr/AgBr hybrid carbon nanofibers as photocatalytic matrerials. The color of RhB solution become amost colorless within 10 min. Compared the decolorization rate of the physical mixture of carbon nanofibers and BiOBr/AgBr hybrids (1:1 in weight), the carbon nanofibers play an important role to decolor RhB which improve the synergistic effects between photolysis and adsorption. The appearance of BiOBr/AgBr hybrids on the surface of carbon nanofibers enlarges its specific surface area due to these nanosheets interweave together to form an open porous structure, and thus, increasing its adsorption capacity. Nitrogen adsorption-desorption isotherms curves (see Fig. S4 in ESI) were carried to further investigate the porous structure of the products. The BiOBr/AgBr hybrid carbon nanofibers have the highest specific surface area compared to that of pure BiOBr and carbon nanofibers, owing to the pore been produced by the association of the smaller nanosheets which has a positive role for improvement of photocatalytic activity. Meanwhile, the pre-enriched RhB molecules can be excited by light, and then the photo-induced electrons inject into the conduction band of BiOBr/AgBr hybrids, triggering the photo-degradation reactions. The stability and reusability of catalysts are very important issues for practical applications. The activity of BiOBr/AgBr hybrid carbon nanofibers is monitored for seven cycles under the same conditions for 20 min after simple separations and dry. As shown in Fig. 5B, no significant change in the photocatalytic activity is observed, indicating durability of our separable photocatalyst in degradation of RhB. It can be seen that the catalyst does not exhibit a significant loss of activity in seven successive runs. The degradation of RhB remains higher than 90% in each cycle, confirming BiOBr/AgBr hybrid carbon nanofibers is not photocorroded and rather stable during the photocatalytic reaction. The excellent reuse performance of the BiOBr/AgBr hybrid carbon nanofibers may be resulted from the good binding property between BiOBr/AgBr hybrid carbon nanofibers layer and carbon nanofibers.

For investigation of plausible reaction mechanism for the superior photocatalytic activity of BiOBr/AgBr hybrid carbon nanofibers and detection the active species during photocatalytic reactivity, hydroxyl radicals (•OH), superoxide radical ($\bullet O_2^-$), and holes (h^+) are investigated by adding 1.0 mM isopropyl alcohol (IPA, a quencher of •OH), p-benzoquinone (BQ, a quencher of $\bullet O_2^-$), and triethanolamine (TEOA, a quencher of h^+), respectively (see detail in ESI) [20]. It can be founded that addition of 1 mM BQ into the reaction system, the decolorization rate of RhB were decelerated significantly compared with addition of 1.0 mM of IPA or TEOA. Therefore, it can be concluded that $\bullet O_2^-$ plays an important role for degradation of organic pollutants solution under light irradiation, as shown in Fig. 5C. When N_2 is bubbled into the reaction system, the degradation of RhB over the BiOBr/AgBr hybrids composite carbon nanofibers is decelerated. However, the degradation of RhB is completely under the same conditions bubbled with O_2.

The phenomena reveal that molecular oxygen has important effect on the photocatalytic degradation of RhB over the BiOBr/AgBr hybrids composite carbon nanofibers [21]. It indicates $\bullet O_2^-$ is even more efficient oxidizers, which result in the oxidation and eventual mineralization of organic compounds [22].

From the analysis above, it can be concluded that the light irradiation activates BiOBr/AgBr hybrids to generate strongly oxidative holes (h^+) in valence band and reductive electrons (e^-) in conduction band. Then, these photo-induced electrons are trapped by dissolved oxygen (O_2) to yield superoxide ions ($\bullet O_2^-$) and H_2O_2 and then to hydroxyl radicals (•OH) [21]. On the other hand, the electron transfer between BiOBr/AgBr hybrids and carbon nanofibers will greatly retard the recombination of photo induced charge carriers and prolong electron lifetime, which may be an important role for the excellent photoactivity of the products [9a,23]. Based on the above results, it can be concluded that photogenerated holes and •OH are the major species active for the photodegradation of RhB, and $\bullet O_2^-$ is just an intermediate to produce •OH but does not involve directly in the degradation of RhB. This well explains the phenomena that the effect of bubbling of N_2 and O_2 into the reacting solution on the photodegradation of RhB is markedly inhibited and enhanced, respectively (Fig. 5D). The role of carbon nanofibers among composite during the photocatalytic reaction can be summarized as follows: (1) as substrate for immobilization of BiOBr/AgBr hybids; (2) as conductor for acceleration of electron transfer; (3) enhancement the synergistic effect between photolysis and adsorption.

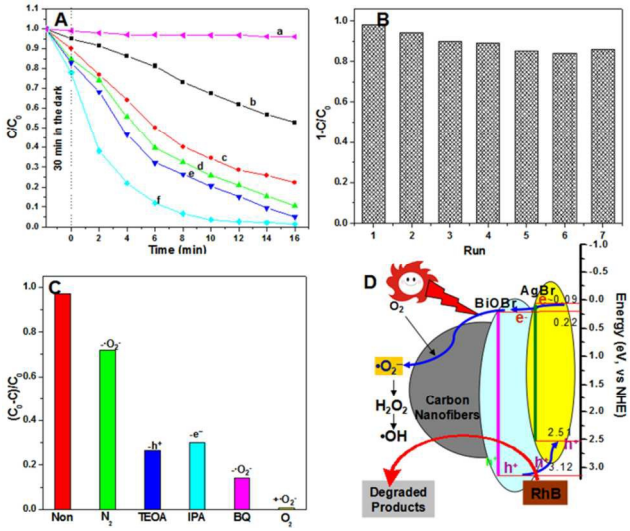

Fig. 5 Photocatalytic degradation of RhB over various products (a: blank, b: carbon nanofibers, c: BiOBr, d: BiOBr/AgBr, e: physical mixture of carbon nanofibers and BiOBr/AgBr hybrids (1:1 in weight); f: BiOBr/AgBr hybrids composite carbon nanofibers) (A) and cycling runs for the photodegradation of RhB over as-prepared BiOBr/AgBr hybrid carbon nanofibers (B). Trapping experiment of active species during the photocatalytic degradation of RhB reaction by addition of 1.0 mM IPA, TEOA or BQ. For the comparison, a blank experiment (without catalysts) and two catalytic experiments (with catalysts) bubbled with N_2 and O_2 are carried out as well (C). Schematic illustration of the photocatalytic mechanism of organic pollutants degradation over N-doped BiOBr/CFs photocatalyst (D).

Conclusions

In summary, the carbon nanofibers have been prepared by carbonization of PAN nanofibers. Then, the BiOBr/AgBr hybrids with flower-like nanosheet structure could be further immobilized on the surface of carbon nanofibers by a facile solvothermal route. The morphologies, structural properties, and photocatalytic activities of the resultant products were investigated. At the same time, it also proves that the final removal of organic pollutants from solutions is caused by photocatalytic degradation rather than by sorption. Furthermore, the three-dimensional (3D) BiOBr/AgBr hybrid structure can capture light from all directions, thus showing potential for application in places with high albedo (high fraction of reflected radiation). This work may provide new insights into preparing other inorganic photocatalytic fibers and may extend their potential applications for degradation of organic pollutants.

Acknowledgements

This work was financially supported by the National Natural Science Foundation of China (51373155, 51133006), Public Technology Research Project of Zhejiang Province (2014C33G2060070) and "521 Talents Training Plan" in Zhejiang Sci-Tech University (ZSTU).

Notes and references

[a] *Department of Materials Engineering, Zhejiang Sci-Tech University, Hangzhou 310018, P. R. China. Tel: +86 571 86843527; E-mail address: ghjiang_cn@zstu.edu.cn (G. Jiang)*

[b] *National Engineering Laboratory for Textile Fiber Materials and Processing Technology (Zhejiang), Hangzhou 310018, P. R. China.*

[c] *Key Laboratory of Advanced Textile Materials and Manufacturing Technology (ATMT), Ministry of Education, Hangzhou 310018, P. R. China.*

†Electronic Supplementary Information (ESI) available: details of materials, preparation of composite carbon nanofibers, preparation of BiOBr/AgBr composite carbon nanofibers, characterization, measurement of photocatalytic activity, SEM images of PAN/$BiCl_3$ composite nanofibers before and after carbonization, SEM images of BiOBr/AgBr hybrid composite carbon nanofibers obtained at different reaction time, N_2 adsorption–desorption isotherms curves. See DOI: 10.1039/b000000x/

1. Z. Liu, Y.-E. Miao, M. Liu, Q. Ding, W. W. Tjiu, X. Cui, T. Liu, *J. Colloid Interface Sci.*, 2014, **424**, 49-55.
2. a) I. K. Konstantinou, T. A. Albanis, *Appl. Catal. B: Environ.*, 2004, **49**, 1-14. b) G. Jiang, X. Li, Z. Wei, T. Jiang, X. Du, W. Chen, *Powder Technol.*, 2014, **260**, 84-89; c) R. Wang, G. Jiang, Y. Ding, Y. Wang, X. Sun, X. Wang, W. Chen, *ACS Appl. Mater. Interfaces*, 2011, **3**, 4154-4158.
3. a) H. Tong, S. Ouyang, Y. Bi, N. Umezawa, M. Oshikiri, J. Ye, *Adv. Mater.*, 2012, **24**, 229-251; b) G. Jiang, X. Wang, Z. Wei, X. Li, X. Xi, R. Hu, B. Tang, R. Wang, S. Wang, T. Wang, W. Chen, *J. Mater. Chem. A*, 2013, **1**, 2406-2410; c) W. Guo, F. Zhang, C. Lin, Z. L. Wang, *Adv. Mater.*, 2012, **24**, 4761-4764.
4. R. Wang, G. Jiang, X. Wang, R. Hu, X. Xi, S. Bao, Y. Zhou, T. Tong, S. Wang, T. Wang, W. Chen, *Powder Technol.*, 2012, **228**, 258-263.
5. a) Z. Ai, W. Ho, S. Lee, L. Zhang, *Environ. Sci. Technol.*, 2009, **43**, 4143-4150; b) M. A. Gondal, X. Chang, M. A. Ali, A. H. Yamani, Q. Zhou, G. Ji, *Appl. Catal. A: Gen.*, 2011, **397**, 192-200; c) H. Cheng, B. Huang, P. Wang, Z. Wang, Z. Lou, J. Wang, X. Qin, X. Zhang, Y. Dai, Chem. Commun., 2011, **47**, 7054-7056; d) Y. Fang, Y. Huang, J. Yang, P. Wang, G. Cheng, Environ. Sci. Technol., 2011, **45**, 1593-1600; e) T. Li, G. Chen, C. Zhou, Z. Shen, R. Jin, J. Sun, *Dalton Trans.*, 2011, **40**, 6751-6758; f) W. Wang, F. Huang, X. Lin, J. Yang, *Catal. Commun.*, 2008, 9, 8-12; g) Y. Feng, L. Li, J. Li, J. Wang, L. Liu, *J. Hazard. Mater.*, 2011, **192**, 538-544.
6. a) Z. Liu, H. Ran, J. Niu, P. Feng, Y. Zhu, *J. Colloid Interface Sci.*, 2014, **431**, 187-193; b) J. Li, Y. Yu, L. Zhang, *Nanoscale*, 2014, **6**, 8473-8488; c) C. Yu, F. Cao, G. Li, R. Wei, J. C. Yu, R. Jin, Q. Fan, C. Wang, *Sep. Purif. Technol.*, 2013, **120**, 110-122.
7. B. F. Dal, S. G. Hardin, D. G. Hay, T. W. Turney, *J. Mater. Sci.*, 1993, **28**, 6657-6664.

8. G. Jiang, R. Wang, X. Wang, R. Hu, X. Xi, Y. Zhou, S. Wang, T. Wang, W. Chen, *ACS Appl. Mater. Interfaces*, 2012, **4**, 4440-4444.
9. a) G. Jiang, X. Li, Z. Wei, T. Jiang, X. Du,W. Chen, *Powder Technol.*, 2014, **260**, 84-89; b) G. Jiang, X. Li, Z.Wei, X.Wang, T. Jiang, X. Du, W. Chen, *Powder Technol.*, 2014, **261**, 170-175; c) J. Zhang, F. Shi, J. Lin, D. Chen, J. Gao, Z. Huang, X. Ding, C. Tang, *Chem. Mater.*, 2008, **20**, 2937-2941; d) G. Jiang, B. Tang, H. Chen, Y. Liu, L. Li, Q. Huang, W. Chen., *RSC Adv.*, 2015, **5**, 25801-25805.
10. a) C. Yu, C. Fan, X. Meng, K. Yang, F. Cao, X. Li, *Reac. Kinet. Mech. Cat.*, 2011, **103**, 141-151. b) L. Lu, L. Kong, Z. Jiang, L. Lu, L. Kong, Z. Jiang, H. H.-C. Lai, T. Xiao, P. P. Edwards, *Catal. Lett.*, 2012, **142**, 771-778.
11. H. Wang, J. Gao, T. Guo, R. Wang, L. Guo, Y. Liu, J. Li, *Chem. Commun.*, 2012, **48**, 275-277.
12. Y. Zhao, Z. Zhang, H. Dang, *Mater. Lett.*, 2004, **58**, 790-793.
13. Z. Jiang, F. Yang, G. Yang, L. Kong, M. O. Jones, T. Xiao, P. P. Edwards, *J. Photochem. Photobio. A:-Chem.*, 2010, **212**, 8-13.
14. a) K.-L. Li, W. W. Lee, C.-S. Lu, Y.-M. Dai, S.-Y. Chou, H.-L. Chen, H.-P. Lin, C.-C. Chen. *J. Taiwan Inst. Chem. Eng.*, 2014, **45**, 2688-2697. b) S. Wang, W. Ma, Y. Fang, M. Jia, Y. Huang. *Appl. Catal. B-Environ.*, 2014, **150-151**, 380-388.
15. L. Zhang, K.-H. Wong, Z. Chen, J. C. Yu, J. Zhao, C. Hu, C.-Y. Chan, P.-K. Wong, *Appl. Catal. A-Gen.*, 2009, **363**, 221-229.
16. X. Bai, L. Wang, Y. Wang, W. Yao, Y. Zhu, *Appl. Catal. B-Environ.*, 2014, **152-153**, 262-270.
17. L. Kong, Z. Jiang, T. Xiao, L. Lu, M. O. Jones, P. P. Edwards, *Chem. Commun.*, 2011, **47**, 5512-5514.
18. X. Tu, S. Luo, G. Chen, J. Li, *Chem. Eur. J.,* 2012, **18**, 14359-14366.
19. J. Shi, H. Cui, J. Chen, M. Fu, B. Xu, H. Luo, Z. Ye. *J. Colloid Interface Sci.* 2012, **388**, 201-208.
20. a) L. Ye, J. Liu, C. Gong. *ACS Catal*., 2012, **2**, 1677-1683. b) L. Chen, S. Yin, S. Luo, *Ind. Eng. Chem. Res*. 2012, **51**, 6760-6768.
21. J. Ma, L.-Z. Zhang, Y.-H. Wang, S.-L. Lei, X.-B. Luo, S.-H. Chen, G.-S. Zeng, J.-P. Zou, S.-L. Luo, C.-T. Au, *Chem. Eng. J.* 2014, **251**, 371-380.
22. a) J. Xiao, Y. Xie, H. Cao. Chemosphere, 2015, **121**, 1-17. b) Y. Li, J. Niu, L. Yin, W. Wang, Y. Bao, J. Chen, Y. Duan. *J. Environ. Sci.*, 2011, **23**, 1911-1918.
23. W. Cui, S. Ma, L. Liu, J. Hu, Y. Liang, J. G. McEvoy. *Appl. Surface Sci.*, 2013, **271**, 171-181.